Physics Letters B 750 (2015) 360–366

Contents lists available at ScienceDirect

Physics Letters B

www.elsevier.com/locate/physletb

Measurement of very forward neutron energy spectra for 7 TeV proton–proton collisions at the Large Hadron Collider

O. Adriani [a,b], E. Berti [a,b], L. Bonechi [a], M. Bongi [a,b], G. Castellini [a,c], R. D'Alessandro [a,b], M. Del Prete [a,b], M. Haguenauer [d], Y. Itow [e,f], K. Kasahara [g], K. Kawade [e,*], Y. Makino [e], K. Masuda [e], E. Matsubayashi [e], H. Menjo [h], G. Mitsuka [b], Y. Muraki [e], Y. Okuno [e], P. Papini [a], A.-L. Perrot [i], S. Ricciarini [a,c], T. Sako [e,f], N. Sakurai [f], Y. Sugiura [e], T. Suzuki [g], T. Tamura [j], A. Tiberio [a,b], S. Torii [g], A. Tricomi [k,l], W.C. Turner [m], Q.D. Zhou [e]

[a] *INFN Section of Florence, Italy*
[b] *University of Florence, Italy*
[c] *IFAC-CNR, Italy*
[d] *Ecole-Polytechnique, France*
[e] *Solar-Terrestrial Environment Laboratory, Nagoya University, Japan*
[f] *Kobayashi-Maskawa Institute for the Origin of Particles and the Universe, Nagoya University, Japan*
[g] *RISE, Waseda University, Japan*
[h] *Graduate School of Science, Nagoya University, Japan*
[i] *CERN, Switzerland*
[j] *Kanagawa University, Japan*
[k] *INFN Section of Catania, Italy*
[l] *University of Catania, Italy*
[m] *LBNL, Berkeley, USA*

ARTICLE INFO

Article history:
Received 13 March 2015
Received in revised form 15 September 2015
Accepted 16 September 2015
Available online 25 September 2015
Editor: M. Doser

Keywords:
LHC
Forward neutron production
Hadronic-interaction model

ABSTRACT

The Large Hadron Collider forward (LHCf) experiment is designed to use the LHC to verify the hadronic-interaction models used in cosmic-ray physics. Forward baryon production is one of the crucial points to understand the development of cosmic-ray showers. We report the neutron-energy spectra for LHC $\sqrt{s} = 7$ TeV proton–proton collisions with the pseudo-rapidity η ranging from 8.81 to 8.99, from 8.99 to 9.22, and from 10.76 to infinity. The measured energy spectra obtained from the two independent calorimeters of Arm1 and Arm2 show the same characteristic feature before unfolding the detector responses. We unfolded the measured spectra by using the multidimensional unfolding method based on Bayesian theory, and the unfolded spectra were compared with current hadronic-interaction models. The QGSJET II-03 model predicts a high neutron production rate at the highest pseudo-rapidity range similar to our results, and the DPMJET 3.04 model describes our results well at the lower pseudo-rapidity ranges. However, no model perfectly explains the experimental results over the entire pseudo-rapidity range. The experimental data indicate a more abundant neutron production rate relative to the photon production than any model predictions studied here.

1. Introduction

The forward particle production process induced by collisions of high-energy particles is a poorly understood phenomenon in high-energy physics. Though it is important to understand the development of cosmic-ray showers in the atmosphere, the validity of hadronic-interaction models has not been sufficiently verified at energies for ultra-high-energy cosmic rays (UHECRs, $> 10^{18}$ eV) because of the lack of experimental data in this energy range. This lack of data results in a large uncertainty in the interpretation of the energy and chemical composition of UHECRs. Forward baryons play a very important role in the development of cosmic-ray showers. If forward baryons carry more collision energy, cosmic-ray showers develop much deeper in the atmosphere, and vice versa. However, in the energy range of UHECRs, the predictions by current models differ significantly among themselves.

* Corresponding author.
E-mail address: kawade@stelab.nagoya-u.ac.jp (K. Kawade).

http://dx.doi.org/10.1016/j.physletb.2015.09.041

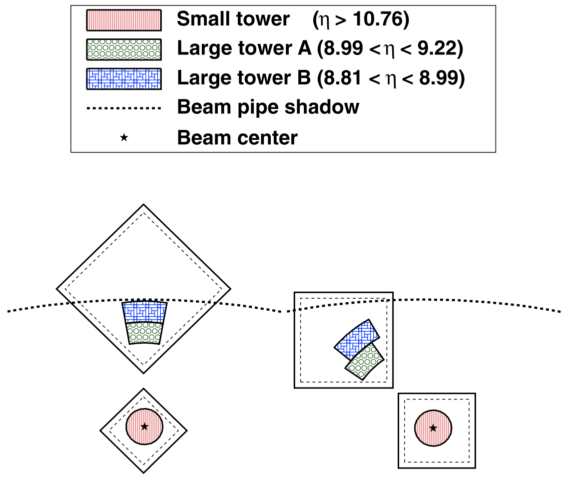

Fig. 1. Cross sections of the LHCf calorimeters (black squares) viewed from IP1. Left and right figures correspond to Arm1 and Arm2, respectively. The three pseudo-rapidity ranges used in the analysis are also indicated. Particles emitted in the direction above the dotted 'Beam pipe shadow' line hit the beam pipe before arriving at the LHCf detectors.

The excess of muons at ground level is reported as one of the problems in the cosmic-ray shower observations. The number of muons observed by the surface detector array of the Pierre Auger Observatory (PAO) [1] is higher than the number expected based on the energy determined by the fluorescence detectors even if a heavy primary mass is assumed [2]. It is suggested that the number of (anti) baryons generated in the forward region is strongly related to the number of muons observed by PAO at the ground [3]. Therefore, baryon production in the very forward region is quite important to understand cosmic-ray showers.

In this paper, we report the results of analyzing the data of the Large Hadron Collider forward (LHCf) experiment for forward neutron spectra. Forward baryon spectra at the fixed-target equivalent energy of 2.5×10^{16} eV ($\sqrt{s} = 7$ TeV) will be a crucial input to improve the hadronic-interaction models used in the air shower analyses.

2. LHCf experiment

The LHCf experiment was designed to use the LHC to verify the hadronic-interaction models used in cosmic-ray experiments [4,5]. Two independent detectors named Arm1 and Arm2 were installed in the detector installation slots of the Target Neutral Absorbers (TAN) located 140 m away from the interaction point 1 (IP1). Because charged particles are swept away by the D1 bending magnets, LHCf can measure only neutral particles in the very forward region of the LHC (pseudo-rapidity $|\eta| > 8.4$). Both detectors have two different sampling calorimeters with 44 radiation lengths (1.6 hadron-interaction lengths) of tungsten plates and 16 layers of sampling scintillators [5]. Four layers of position sensors (SciFi in Arm1 and silicon micro-strip sensors in Arm2) can measure the hit position transverse to the beam direction. The transverse dimensions of the calorimeters are 20 mm × 20 mm and 40 mm × 40 mm in Arm1, and 25 mm × 25 mm and 32 mm × 32 mm in Arm2. The cross sections of the calorimeters viewed from IP1 are shown in Fig. 1. The calorimeter with the smaller (larger) dimensions in each Arm is referred to as the 'small (large) tower' hereafter. The small towers covered the zero degree emission angle of the neutral particles as indicated by stars in Fig. 1. The details of the detector performance during the 2009–2010 proton–proton collisions are reported in [6].

The performance of the LHCf detectors for hadron measurements was studied by Monte Carlo (MC) simulations and confirmed by using 350 GeV proton beams at CERN-SPS [7]. Depending on the incident-neutron energy, the energy resolution and position resolution are about 40% and 0.1–1.3 mm, respectively. The detection efficiency for neutrons was estimated to be 70%–80% for neutrons above 500 GeV.

In this paper we assume hadronic showers are produced by neutrons. Depending on the generators used in this paper, 0–6% of other hadrons, i.e., Λs and K^0s, are also included in the data.

3. Analysis

3.1. Data used in the analysis

The data used in this analysis were obtained on May 15, 2010 from proton–proton collisions at $\sqrt{s} = 7$ TeV (LHC Fill # 1104). The typical luminosity corresponding to this fill derived from the counting rate of the LHCf front counters [8] was (6.3–6.5) × 10^{28} $\mathrm{cm}^{-2}\ \mathrm{s}^{-1}$. The data set was the same as the one used in the previously published photon analysis results, and additional details can be found in [9]. The trigger for LHCf events was generated when signals from any three successive scintillation layers in any calorimeter exceeded a predefined threshold (typically 130 minimum ionizing particles (MIPs)). Data acquisition (DAQ) was performed with an average efficiency of 85.7% (Arm1) and 67.0% (Arm2).

Taking the DAQ efficiency into account, the integrated luminosities of the data set were 0.68 nb^{-1} for Arm1 and 0.53 nb^{-1} for Arm2, each with ±6.1% uncertainty. The numbers of inelastic collisions were about 48M and 38M collisions for Arm1 and Arm2, respectively.

MC predictions were conducted with the generators DPMJET 3.04 [10], EPOS 1.99 [11], PYTHIA 8.145 [12], QGSJET II-03 [13], and SYBILL 2.1 [14] and compared with the experimental results. In the MC simulations, the COSMOS (v7.49) and EPICS (v8.81) [15] libraries that are used in air-shower and detector simulations were used to simulate the flight of particles from the IP1 to the detectors and the response of the detectors. About 10M inelastic collisions were simulated for each model.

3.2. Event reconstruction

Initially, the offline-event selection was applied when energy depositions equivalent to more than 200 MIPs were recorded for three successive layers in addition to the experimental trigger. The positions at which particles hit the detector were determined by using the position sensors. Because reconstruction of the events is difficult at the edge of the calorimeters due to large fluctuations in the energy deposition, events within 2 mm from the edge were discarded from the analysis (dashed squares in Fig. 1). The lateral shower leakage caused by the limited lateral size of the detectors degrades the energy resolution. This position-dependent leakage effect was corrected as a function of the transverse-hit position measured by the position sensors.

Particle identification (PID) between neutrons and photons was based on the difference in the longitudinal shape of the shower development. Two simple parameters called $L_{20\%}$ and $L_{90\%}$ were introduced to characterize the shower shape. These parameters were defined as the depths in radiation length containing 20% and 90%, respectively, of the total energy deposited within the layers. Considering the correlation between $L_{20\%}$ and $L_{90\%}$ an optimized parameter $\mathrm{L_{2D}}$ was defined as $\mathrm{L_{2D}} = L_{90\%} - 1/4 \times L_{20\%}$ to improve the selection efficiency and purity compared to previous analyses.

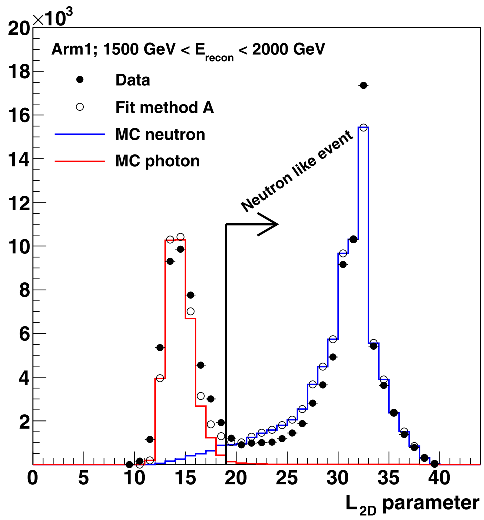

Fig. 2. The L_{2D} parameter distribution for the experimental data and the MC simulations from the template MC. The closed circles represent the Arm1 experimental results, whereas the red and blue histograms correspond to photon and neutron predictions. The open circles are the scaled results of the MC simulation obtained by Method A. (For interpretation of the references to color in this figure legend, the reader is referred to the web version of this article.)

Fig. 2 shows the L_{2D} distributions. Two distinct peaks are identified in the observed L_{2D} distribution indicated by the closed circles. The histograms correspond to the MC prediction of pure photons (red) and pure neutrons (blue) scaled to the data, and they are referred to as 'templates' hereafter. The templates were produced by accumulating the MC simulation as a mixture of five models, DPMJET 3.04, EPOS 1.99, PYTHIA 8.145, QGSJET II-03, and SYBILL 2.1, with same statistics for each. This was performed to increase the number of events for simulating the detector response. Differences in the input models do not impact the shape of templates.

To obtain neutron spectra, only events with the parameter L_{2D} exceeding a certain threshold were identified as neutron-like events. The effects of the neutron selection efficiency and the photon contamination were corrected by using the efficiency ϵ and purity P (i.e., multiplying by P/ϵ) determined by MC simulations and the template fitting method [6,9,16], respectively. To estimate the photon contamination, the templates for photons and hadrons were independently scaled to reproduce the experimental results (referred to as Method A). The open circles in Fig. 2 represent the fitting result with Method A. Neutron selection criteria, as indicated in Fig. 2, were chosen to maximize $\epsilon \times P$. To cope with energy dependence, determinations of the PID threshold and correction factors, P and ϵ, were performed in eight different energy ranges according to reconstructed energy.

After correcting the PID efficiency and purity, we obtained the production rate of neutrons as a function of obtained energy that was determined from the total deposited energy in the calorimeter and from the identity of the particle. Details of the event reconstruction for neutrons are summarized in [7]. About 0.3 million neutron-like events passed the PID selection for each arm.

To combine the results of Arm1 and Arm2, we selected events that occurred within the common rapidity regions as indicated in Fig. 1. Events within 6 mm ($\eta > 10.76$) from the beam center were selected for the small towers. The large towers of Arm1 and Arm2 were divided into two regions. The inner region "A" was defined by a radius of 28–35 mm ($8.99 < \eta < 9.22$) from the beam center, whereas the outer region "B" was defined by a radius of 35–42 mm ($8.81 < \eta < 8.99$). For the analysis, we used azimuthal-angle intervals $d\phi$ of 360° for the small towers and 20° for the large towers.

3.3. Systematic uncertainties

Energy scale

In order to determine the energy scale and estimate its systematic uncertainty, we followed the previous analyses [9,17]. An analysis of the reconstructed invariant mass in π^0 decays indicated mass excesses of 8.1% (Arm1) and 3.7% (Arm2) compared with the π^0 mass reconstructed in the MC simulations. These excesses were attributed to the miscalibration of the energy scale and the energy scales were corrected in this analysis. Based on this mass excess correction and known calibration uncertainty, in total, values of ±5.6% (Arm1) and ±4.4% (Arm2) were assigned to be the systematic uncertainty with respect to the central value of the mass shift. In addition, according to the differences between the SPS beam test and MC simulation in the reconstructed energy of 350 GeV proton showers [7], +2.0% (Arm1) and −3.8% (Arm2) errors were added quadratically to the respective energy scale uncertainties.

PID

Method A described in Section 3.2 did not perfectly reproduce the experimental results. To estimate systematic effects from these differences, we used a more artificial method (Method B) that allows longitudinal displacements and modifications in the width of the distributions until the experimental results are matched [18]. The systematic uncertainty from the PID process was estimated by comparing the results using the Method A and Method B. The energy-dependent PID systematic uncertainty is at most 1% above 1.5 TeV and at most 12% below this energy.

The relative differences in the neutron production rate defined as

$$1 - \frac{P_B/\epsilon_B}{P_A/\epsilon_A} \quad (1)$$

are summarized in Table 1. Here, ϵ_A (ϵ_B) and P_A (P_B) are the efficiency and purity determined by Method A (Method B), respectively. Final results are given using the Method A, while the differences shown in Table 1 are taken as a part of the systematic uncertainties.

Multi-hit

When two or more particles enter one of the LHCf calorimeters, these events are called 'multihit' events. Because discriminating between single and multihit events for neutron-like events was difficult due to the large fluctuation of hadronic showers, rejection

Table 1
Relative differences in eight bin energy spectra to evaluate systematic uncertainties from the PID process. Small tower, Large tower A, and Large tower B correspond to the rapidity ranges from 10.76 to infinity, from 8.99 to 9.22, and from 8.82 to 8.99, respectively.

LHCf Energy [GeV]	100–500	500–1000	1000–1500	1500–2000	2000–2500	2500–3000	3000–3500	3500<
Small tower	8.0%	3.6%	2.0%	1.3%	0.7%	0.8%	0.8%	4.2%
Large tower A	13.9%	10.4%	4.8%	2.6%	1.8%	2.0%	2.3%	11.0%
Large tower B	17.7%	12.2%	4.1%	2.0%	1.9%	2.2%	3.0%	22.2%

Table 2
Relative differences of ten bin energy spectra to evaluate systematic error from multihit events. Small tower, Large tower A, and Large tower B correspond to the rapidity ranges from 10.76 to infinity, from 8.99 to 9.22, and from 8.82 to 8.99, respectively.

LHCf Energy [GeV]	100–500	500–1000	1000–1500	1500–2000	2000–2500	2500–3000	3000–3500	3500–4000	4000–5000	5000<
Small tower	18.1%	5.9%	2.6%	2.0%	2.0%	2.2%	2.4%	3.8%	3.6%	5.5%
Large tower A	9.9%	6.1%	3.7%	4.1%	4.8%	5.7%	7.1%	9.6%	10.0%	15.5%
Large tower B	9.3%	3.9%	3.9%	4.4%	5.3%	7.9%	9.2%	12.2%	14.5%	–

Table 3
Relative differences in eight bin energy spectra to evaluate systematic error due to position resolution. Small tower, Large tower A, and Large tower B correspond to the rapidity ranges from 10.76 to infinity, from 8.99 to 9.22, and from 8.82 to 8.99, respectively.

LHCf Energy [GeV]	100–500	500–1000	1000–1500	1500–2000	2000–2500	2500–3000	3000–3500	3500<
Small tower	23.2%	8.4%	4.5%	3.9%	2.5%	2.4%	1.9%	2.0%
Large tower A	54.2%	1.0%	0.9%	2.5%	0.6%	3.3%	3.6%	5.0%
Large tower B	11.0%	0.0%	1.4%	0.6%	1.1%	1.0%	3.7%	5.7%

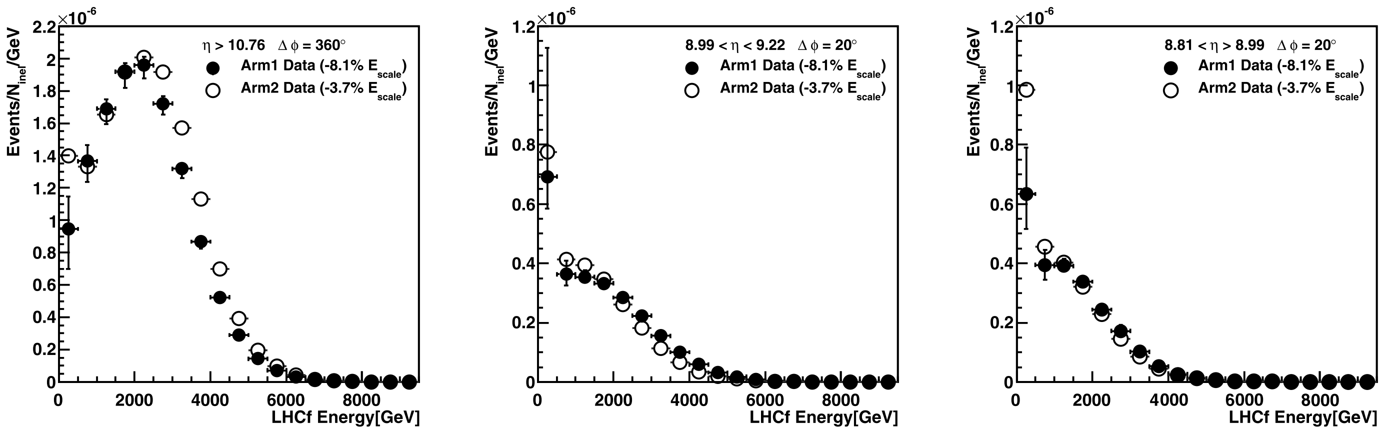

Fig. 3. Energy spectra of neutron-like events measured by the Arm1 and Arm2 detectors. The left panel shows the results from the small towers, and the center and right panels show the results for the large towers. The horizontal axes represent the reconstructed energy. The vertical bars represent the statistical (they are negligibly small) and systematic uncertainties (excluding the energy scale and the luminosity uncertainties).

of multihit events causes a large systematic uncertainty. Because the multihit event rate was predicted by MC simulations to be less than a few percent, all events used for this analysis were treated as single-hit events. The systematic effects on the energy spectra from multihit events were studied by using MC simulations. We tested the difference between the spectra with the current method and those with ideal multihit reconstruction by using the MC study. The difference was less than 6% above 500 GeV, as summarized in Table 2, and was taken into account as a part of the systematic uncertainties.

Position resolution

Because the resolution of the transverse hit position for neutrons is 0.1–1.3 mm depending on the neutron energy [7], some events were reconstructed as hits at positions far from the true hit position. Thus particles hitting outside of the fiducial area may migrate into the fiducial area and vice versa. The effect of the position resolution was estimated by using MC simulations.

The differences between neutron-energy spectra selected by the reconstructed position and the true hit positions were calculated with EPOS 1.99, QGSJET II-03, SYBILL 2.1, DPMJET 3.04, and PYTHIA 8.145. Because no significant model dependence was found, the average of the predictions by the five different models was assigned to the systematic uncertainty. The systematic error from these effects was less than 8.4% at energies above 500 GeV, as summarized in Table 3.

Other systematic errors

Similar to the previous study [9], the other systematic errors, such as the integrated luminosity ($\pm$6.1%) and position of the beam center (typically $\pm$3–10%) were taken into account. The systematic uncertainty from pile-up events (0.2%) was negligibly small.

4. Results

4.1. Measured energy spectra

Fig. 3 shows the energy spectra of forward neutrons measured by the LHCf Arm1 and LHCf Arm2 detectors. The energy scale correction described above was applied in these spectra ($-$8.1% for Arm1 and $-$3.7% for Arm2). The vertical axes were normalized to the number of inelastic collisions per GeV. The vertical bars represent the statistical uncertainties (which are very small) and systematic uncertainties (excluding the energy scale and luminosity uncertainties).[1] The closed and open circles show the results of the Arm1 and Arm2 detectors, respectively. A small difference in the detection efficiencies of the Arm1 and Arm2 detectors was not corrected here because it is treated in the unfolding process discussed in Section 4.2. In spite of the difference in detector re-

[1] The uncertainty due to the luminosity determination is not indicated in the figures throughout this paper.

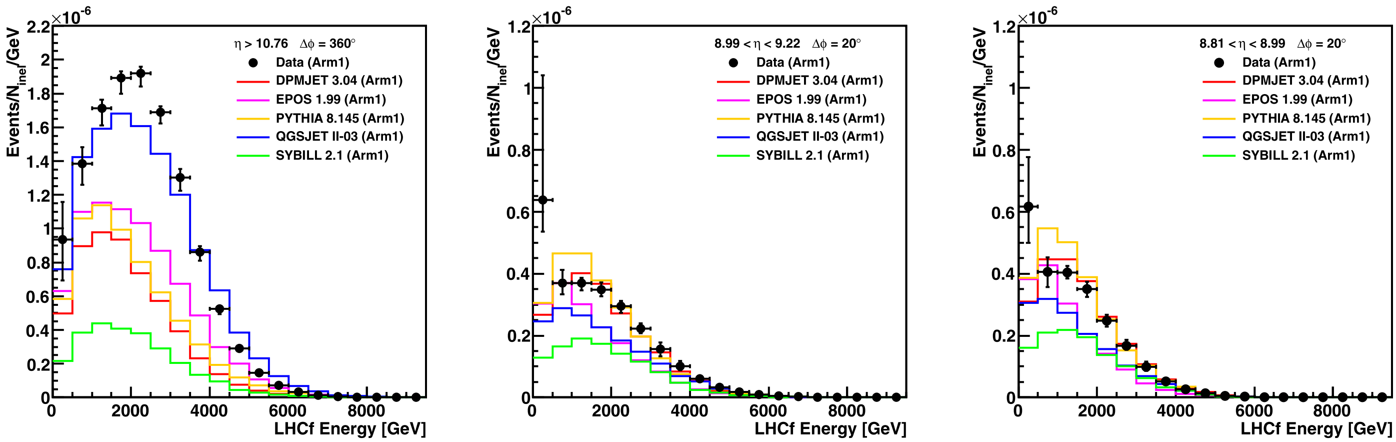

Fig. 4. Measured Arm1 energy spectra of neutron-like events together with MC predictions. The left panel shows the results for the small tower, and the center and right panels show the results for the large tower. The vertical bars represent the statistical uncertainties (which are very small) and systematic uncertainties (excluding the energy scale and luminosity uncertainties). Colored lines indicate MC predictions by EPOS 1.99 (magenta), QGSJET II-03 (blue), SYBILL 2.1 (green), DPMJET 3.04 (red), and PYTHIA 8.145 (yellow). (For interpretation of the references to color in this figure legend, the reader is referred to the web version of this article.)

sponse, data from both arms show the same characteristic feature of the spectra.

Fig. 4 compares the energy spectra measured by the Arm1 detector with the MC predictions. Colored lines indicate MC predictions by EPOS 1.99 (magenta), QGSJET II-03 (blue), SYBILL 2.1 (green), DPMJET 3.04 (red), and PYTHIA 8.145 (yellow). The model spectra were obtained from full detector simulations taking account of the same reconstruction process as the experimental data. None of the models perfectly matches the experimental data. The experimental results are close to the model predictions showing the most abundant neutron production.

4.2. Spectra unfolding

To estimate the true energy distribution, we used the multi-dimensional-spectra unfolding method [19] with variables energy and transverse momentum (p_T). To create training samples for the unfolding process, we used MC simulations with neutrons having a flat energy spectrum from 50 to 3500 GeV and a uniform injection into the detector plane. The training samples were reconstructed by using the same method as the experimental data. The performance of the unfolding method was checked by applying the unfolding process to the MC spectra and comparing the results with the true spectra. The unfolding process was applied iteratively until the result converged at the 4th iteration.

The upper panel in Fig. 5 shows the unfolded spectra for the DPMJET 3.04 and EPOS 1.99 models together with the true spectra at the small tower of Arm1. Here, “true spectra” indicate the true neutron energy distributions of the MC events after acceptance and trigger threshold were applied. The bottom panel shows the ratio of the unfolded spectra to the true spectra. The differences between the unfolded and true spectra were mostly within 20% except in the highest energy bins (50–100%). These systematic differences were due to the choice of the flat energy distribution as a training sample. We found that the difference did not strongly differ among the five input models. Thus, we applied another correction by dividing the unfolded spectra by the average of the differences. The differences among the five models, typically ±10%, were considered as a part of the systematic uncertainties.

Fig. 6 shows the unfolded experimental spectra measured by the Arm1 and Arm2 detectors for each rapidity range. The shaded areas show the Arm1 systematic errors, and the bars represent the Arm2 systematic errors. The detection efficiency of neutrons and

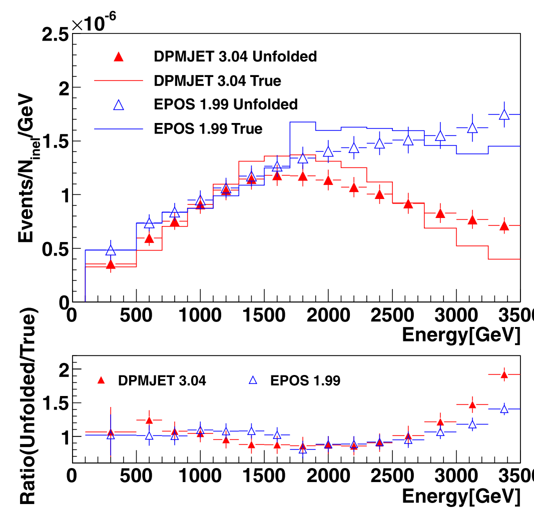

Fig. 5. Comparison of unfolded spectra with true spectra for the DPMJET 3.04 and EPOS 1.99 models at the small tower of Arm1. The bottom panel shows the ratio of the unfolded spectra to the true spectra. (For interpretation of the colors in this figure, the reader is referred to the web version of this article.)

the correction in the PID efficiency and purity were also considered. The results below 500 GeV are not shown because of the large systematic errors. The unfolded spectra from both Arms show good agreement within systematic errors.

The experimental spectra were combined according to the previously used method [17]. It was assumed that the systematic uncertainties caused by the energy scale, PID correction, beam center position, multihit events, and position resolution had bin-to-bin correlations while the other elements were independent between bins. The systematic uncertainties except in the unfolding processes were thought to be fully uncorrelated between Arm1 and Arm2. Because we treated the systematic uncertainties of the unfolding processes identically in Arm1 and Arm2, these errors were added quadratically after the combining process.

The differential neutron production cross sections $d\sigma_n/dE$ were calculated from the unfolded experimental spectra by using

$$d\sigma_n/dE = \frac{dN(\Delta\eta, \Delta E)}{\Delta E}\frac{1}{L} \times \frac{2\pi}{d\phi}, \qquad (2)$$

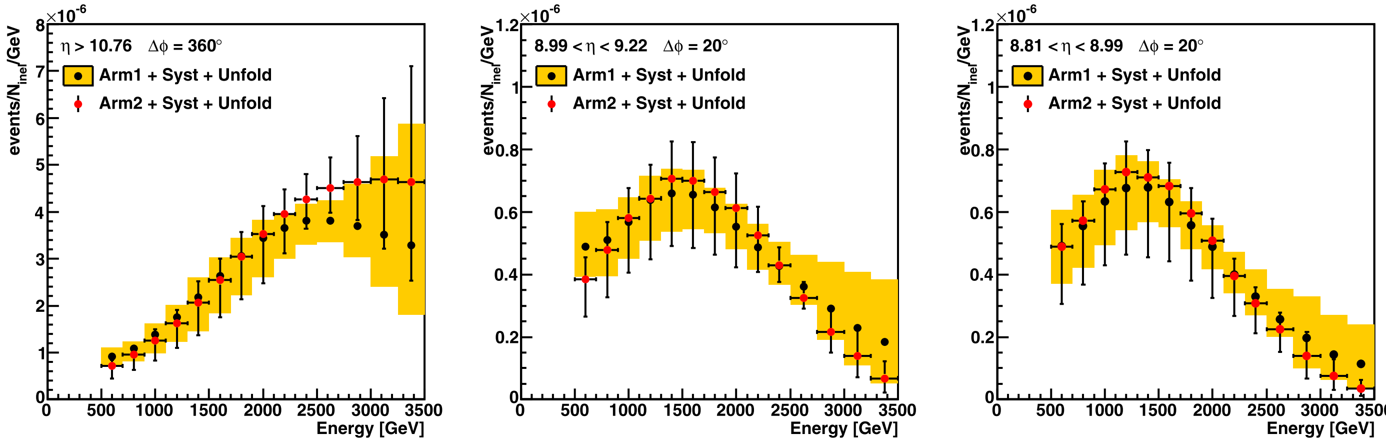

Fig. 6. Unfolded energy spectra of the small towers ($\eta > 10.76$) and the large towers ($8.99 < \eta < 9.22$ and $8.81 < \eta < 8.99$). The yellow shaded areas show the Arm1 systematic errors, and the bars represent the Arm2 systematic errors except the luminosity uncertainty. (For interpretation of the references to color in this figure legend, the reader is referred to the web version of this article.)

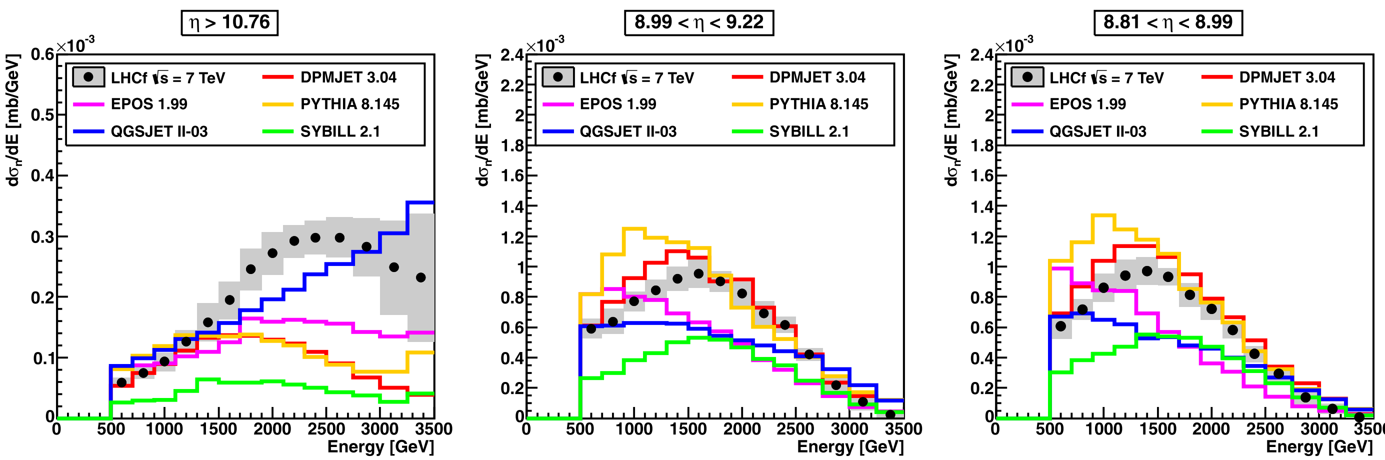

Fig. 7. Comparison of the LHCf results with model predictions at the small tower ($\eta > 10.76$) and large towers ($8.99 < \eta < 9.22$ and $8.81 < \eta < 8.99$). The black markers and gray shaded areas show the combined results of the LHCf Arm1 and Arm2 detectors and the systematic errors, respectively. (For interpretation of the colors in this figure, the reader is referred to the web version of this article.)

where $dN(\Delta\eta, \Delta E)$ is the number of neutrons observed in the each rapidity range, $\Delta\eta$, and each energy bin, ΔE. L is the integrated luminosity corresponding to the data set. The cross sections are summarized in Table 5. Fig. 7 shows the combined Arm1 and Arm2 spectra together with the model predictions. The experimental results indicate the highest neutron production rate compared with the MC models at the most forward rapidity. The QGSJET II-03 model predicts a neutron production rate similar to the experimental results in the largest rapidity range. However, the DPMJET 3.04 model predicts neutron production rates better in the smaller rapidity ranges. These tendencies were already found in the spectra before unfolding, and they are not artifacts of unfolding.

The neutron-to-photon ratios (N_n/N_γ) in three different rapidity regions were extracted after unfolding and are summarized in Table 4. Here, N_n and N_γ are the number of neutrons and number of photons, respectively, with energies greater than 100 GeV. The numbers of photons were obtained from the previous analysis [9] and the same analysis for the pseudo-rapidity range of 8.99–9.22 defined in this study. The experimental data indicate a more abundant neutron production rate relative to the photon production than any model predictions studied here.

Table 4
Hadron-to-photon ratio for experiment and MC models. The number of neutrons with energies above 100 GeV was divided by the number of photons with energies above 100 GeV. The rapidity intervals corresponding to the small tower, Large tower A, and Large tower B are $\eta > 10.76$, $9.22 > \eta > 8.99$, and $8.99 > \eta > 8.81$, respectively.

N_n/N_γ	Small	Large A	Large B
Data	3.05 ± 0.19	1.26 ± 0.08	1.10 ± 0.07
DPMJET 3.04	1.05	0.76	0.74
EPOS 1.99	1.80	0.69	0.63
PYTHIA 8.145	1.27	0.82	0.79
QGSJET II-03	2.34	0.65	0.56
SYBILL 2.1	0.88	0.57	0.53

5. Summary and discussion

An initial analysis of neutron spectra at the very forward region of the LHC is presented in this paper. The data were acquired in May 2010 at the LHC from $\sqrt{s} = 7$ TeV proton–proton collisions with integrated luminosities of 0.68 nb^{-1} and 0.53 nb^{-1} for the LHCf Arm1 and Arm2 detectors, respectively.

The neutron energy spectra were analyzed in three different rapidity regions. The results obtained from the two independent calorimeters of Arm1 and Arm2 are consistent with each other. The measured spectra were combined and unfolded by using a two-dimensional unfolding method based on Bayesian theory. Unavoidable contamination from non-neutron hadrons was not corrected in this analysis. According to the models, about 0–6% of other hadrons are included and this fraction and the energy dependence are model-dependent.

The experimental results, both in folded and unfolded spectra were compared with the MC predictions of QGSJET II-03, EPOS 1.99, DPMJET 3.04, PYTHIA 8.145, and SYBILL 2.1; however, no model perfectly reproduced the experimental results over the entire pseudo-rapidity range. Moreover, compared with the hadronic-interaction models, the experimental results show a more abundant neutron production relative to the photon production rate.

The total energy carried by neutrons integrated over the energy spectrum is larger in the lower rapidity region. EPOS and QGSJET II,[2] current standard models for the air shower analysis, underestimate the neutron production by about 30% in the lower rapidity regions. It is interesting to investigate how these differences affect the development of air showers.

The differential cross sections for neutron production at very forward rapidity were measured at the Intersecting Storage Ring for proton–proton collisions at $\sqrt{s} = 30.6$–62.7 GeV [20,21] and by the PHENIX experiment at the Relativistic Heavy Ion Collider for proton–proton collisions at $\sqrt{s} = 200$ GeV [22]. The results of previous experiments were consistent with Feynman x (x_F) scaling and do not depend on the collision energy. To accurately extrapolate the hadronic-interaction models to the high-energy range (independently of whether or not the x_F scaling in the neutron production is still relevant at energies in the TeV range) is also an important issue. LHCf will extend the energy range to test the Feynman scaling with the proton–proton collision data obtained at $\sqrt{s} = 0.9, 2.76, 7,$ and 13 TeV.

Acknowledgements

We would like to express our gratitude to the CERN staff for their essential contribution to the operation of LHCf. This study was supported by Grant-in-Aids for Scientific Research by MEXT of Japan (grants 26247037 and 23740183), by the Grant-in-Aid for Nagoya University GCOE "QFPU" from MEXT (grant 23244050), and by the Istituto Nazionale di Fisica Nucleare (INFN) in Italy. Part of this work was performed using computer resources provided by the Institute for Cosmic-Ray Research at the University of Tokyo and by CERN.

[2] EPOS-LHC and QGSJET II-04 are the updated versions tuned with the initial LHC data. However the forward particle spectra do not appear to differ from the model spectra shown in this paper.

Appendix A. Cross section table

Table 5
Differential neutron production rate $d\sigma_n/dE$ [mb/GeV] for each rapidity range.

Energy [GeV]	Cross section [mb/GeV] Small tower ($\eta > 10.76$)	Large tower A ($8.99 < \eta < 9.22$)	Large tower B ($8.81 < \eta < 8.99$)
500–700	$(5.91 \pm 0.81) \times 10^{-5}$	$(5.91 \pm 0.66) \times 10^{-4}$	$(6.09 \pm 0.84) \times 10^{-4}$
700–900	$(7.48 \pm 0.95) \times 10^{-5}$	$(6.38 \pm 0.82) \times 10^{-4}$	$(7.15 \pm 0.67) \times 10^{-4}$
900–1100	$(9.32 \pm 1.54) \times 10^{-5}$	$(7.70 \pm 0.66) \times 10^{-4}$	$(8.60 \pm 0.92) \times 10^{-4}$
1100–1300	$(1.26 \pm 0.19) \times 10^{-4}$	$(8.41 \pm 0.75) \times 10^{-4}$	$(9.42 \pm 1.05) \times 10^{-4}$
1300–1500	$(1.58 \pm 0.32) \times 10^{-4}$	$(9.18 \pm 0.80) \times 10^{-4}$	$(9.71 \pm 0.91) \times 10^{-4}$
1500–1700	$(1.95 \pm 0.31) \times 10^{-4}$	$(9.54 \pm 0.92) \times 10^{-4}$	$(9.34 \pm 0.59) \times 10^{-4}$
1700–1900	$(2.45 \pm 0.35) \times 10^{-4}$	$(9.03 \pm 0.68) \times 10^{-4}$	$(8.12 \pm 0.78) \times 10^{-4}$
1900–2100	$(2.72 \pm 0.36) \times 10^{-4}$	$(8.21 \pm 0.81) \times 10^{-4}$	$(7.19 \pm 0.68) \times 10^{-4}$
2100–2300	$(2.92 \pm 0.27) \times 10^{-4}$	$(6.90 \pm 0.82) \times 10^{-4}$	$(5.81 \pm 0.55) \times 10^{-4}$
2300–2500	$(2.98 \pm 0.28) \times 10^{-4}$	$(6.17 \pm 0.52) \times 10^{-4}$	$(4.25 \pm 0.53) \times 10^{-4}$
2500–2750	$(2.98 \pm 0.34) \times 10^{-4}$	$(4.21 \pm 0.44) \times 10^{-4}$	$(2.94 \pm 0.54) \times 10^{-4}$
2750–3000	$(2.82 \pm 0.48) \times 10^{-4}$	$(2.20 \pm 0.68) \times 10^{-4}$	$(1.39 \pm 0.65) \times 10^{-4}$
3000–3250	$(2.49 \pm 0.78) \times 10^{-4}$	$(1.10 \pm 0.55) \times 10^{-4}$	$(6.07 \pm 3.39) \times 10^{-5}$
3250–3500	$(2.32 \pm 1.06) \times 10^{-4}$	$(2.45 \pm 1.70) \times 10^{-5}$	$(5.75 \pm 3.76) \times 10^{-6}$

References

[1] J. Abraham, et al., Phys. Rev. Lett. 101 (2008) 061101.
[2] J. Allen, et al., Proceedings of 32nd ICRC, 2011, Beijin.
[3] T. Pierog, K. Werner, Phys. Rev. Lett. 101 (2008) 171101.
[4] O. Adriani, et al., LHCf-TDR, CERN-LHCC-2006-004.
[5] O. Adriani, et al., J. Instrum. 3 (2008) S08006.
[6] O. Adriani, et al., Int. J. Mod. Phys. A 28 (2013) 1330036.
[7] K. Kawade, et al., J. Instrum. 9 (2014) P03016.
[8] K. Taki, et al., J. Instrum. 7 (2012) T01003.
[9] O. Adriani, et al., Phys. Lett. B 703 (2011) 128.
[10] F.W. Bopp, J. Ranft, R. Engel, S. Roesler, Phys. Rev. C 77 (2008) 014904.
[11] K. Werner, F.M. Liu, T. Pierog, Phys. Rev. C 74 (2006) 044902.
[12] T. Sjöostand, S. Mrenna, P. Skands, Comput. Phys. Commun. 178 (2008) 852.
[13] S. Ostapchenko, Phys. Rev. D 74 (2006) 014026.
[14] E.-J. Ahn, R. Engel, T.K. Gaisser, P. Lipari, T. Stanev, Phys. Rev. D 80 (2009) 094003.
[15] K. Kasahara, EPICS web page, http://cosmos.n.kanagawa-u.ac.jp/.
[16] R. Barlow, C. Beeston, Comput. Phys. Commun. 77 (1993) 219–228.
[17] O. Adriani, et al., Phys. Rev. D 86 (2012) 092001.
[18] K. Kawade, PhD thesis, Nagoya University, 2014, CERN-THESIS-2014-315.
[19] G. D' Agostini, Nucl. Instrum. Meth. A 362 (1995) 487.
[20] J. Engler, et al., Nucl. Phys. B 84 (1975) 70.
[21] W. Flauger, F. Mönnig, Nucl. Phys. B 109 (1976) 347–356.
[22] A. Adare, et al., Phys. Rev. D 88 (2013) 032006.